Studies on plant cell toxicity of luminescent silica nanoparticles (Cs2[Mo6Br14]@SiO2) and its constitutive components

Francisco Cabello-Hurtado, Maria Dolorès Lozano-Baena, Chrystelle Neaime, Agnès Burel, Sylvie Jeanne, Pascal Pellen-Mussi, Stéphane Cordier, Fabien Grasset

Journal of Nanoparticle Research
--Manuscript Preprint--

Studies on plant cell toxicity of luminescent silica nanoparticles ($Cs_2[Mo_6Br_{14}]@SiO_2$) and its constitutive components

Francisco Cabello-Hurtado [a,], María Dolores Lozano-Baena [a], Chrystelle Neaime [b], Agnès Burel [c], Sylvie Jeanne [b], Pascal Pellen-Mussi [b], Stéphane Cordier [b], Fabien Grasset [b, d]*

[a] UMR UR1-CNRS 6553 ECOBIO, Mechanisms at the Origin of Biodiversity Team, University of Rennes 1, 263 av. du Général Leclerc, 35042 Rennes, France

[b] UMR UR1-CNRS 6226 Institut des Sciences Chimiques de Rennes, Solid State Chemistry and Materials Group, University of Rennes 1, 263 av. du Général Leclerc, 35042 Rennes, France

[c] Electronic Microscopy Department, University of Rennes 1, 2 av. du Professeur Léon-Bernard, Campus de Villejean, 35043 Rennes, France

[d] CNRS-Saint Gobain, UMI 3629, Laboratory for Innovative Key Materials and Structures-Link, National Institute of Material Science (NIMS), GREEN/MANA Room 512, 1-1 Namiki, 305-0044 Tsukuba, Japan

* Corresponding author: e-mail: francisco.cabello@univ-rennes1.fr; phone: +33223235022; fax: +33223235026

Acknowledgment

This work was supported by the French National Research Agency (Project CLUSTOP 2011 BS0801301). Authors thank Marie Thérèse Lavault for technical assistance (MRic, UR 1), Juan B. Arellano for kindly providing *Arabidopsis* cells (IRNASA-CSIC), and Vincent Dorcet for nanoparticle TEM microcraphs (Plateforme THEMIS, UR1).

Abstract

As part of the risk evaluation before potential applications of nanomaterials, phytotoxicity of newly designed multifunctional silica nanoparticles (CMB@SiO_2, average diameter of 47 nm) and their components, i.e. molybdenum octahedral cluster bromide units (CMB, 1 nm) and SiO_2 nanoparticles (nSiO_2, 29 nm), has been studied using photosynthetic *Arabidopsis thaliana* cell suspension cultures. CMB clusters presented toxic effects on plant cells, inhibiting cell growth and negatively affecting cell viability and photosynthetic efficiency. Nevertheless, we showed that neither nSiO_2 nor CMB@SiO_2 have any significant effect on cell growth and viability or photosynthetic efficiency. At least part of the harmful impact of CMB clusters could be ascribed to their capacity to generate an oxidative stress since lipid peroxidation greatly increased after CMB exposure, which was not the case for nSiO_2 or CMB@SiO_2 treatments. Exposure of cells to CMB clusters also lead to the induction of several enzymatic antioxidant activities (i.e. superoxide dismutase, guaiacol peroxidase, glutathione peroxidase, glutathione reductase, and glutathione S-transferase activities) compared to control and the other treatments. Finally, using electron microscopy, we showed that *Arabidopsis* cells internalize CMB clusters and both silica nanoparticles, the latter through, most likely, endocytosis-like pathway as nanoparticles were mainly found incorporated into vesicles.

Keywords

Nanotoxicity; Silica nanoparticles; Molybdenum clusters; *Arabidopsis* cells; Oxidative stress.

Introduction

Manufactured nanoparticles (NPs) (one dimension < 100 nm) are being increasingly produced for a wide range of applications and are present in hundreds of nanotechnology products (Buzea et al. 2007). However, they are also bringing new toxic effects on human and environmental health (Buzea et al. 2007; Colvin 2003). Among nanomaterials, the use of functional synthetic amorphous silicon dioxide or silica nanoparticles ($nSiO_2$) in information technology, biotechnology and medicine is becoming increasingly accepted for a variety of therapeutic, diagnostic and imaging applications (Selvan et al. 2010). The challenge for nanotechnologies at this point is to elaborate non-toxic and aging resistant phosphorescent silica nanoparticles emitting in the near infrared region (NIR). For this purpose, new functional silica nanoparticles incorporating luminescent molybdenum hexanuclear cluster bromide units ($Cs_2Mo_6Br_{14}$, noted CMB, as the cluster precursor) inside monodispersed and size-controlled silica nanoparticles (noted CMB@SiO_2) have been recently developed in our group (Aubert et al. 2013). Besides, Mo_6-based clusters are already involved in several patents for applications in biotechnology as contrast agents (Long et al. 1998), oxygen sensors (Baker et al. 2010) and in display technologies (Cordier et al. 2015).

Silica nanoparticles are used as matrices because of their versatility and their relative biocompatibility (Fruijtier-Pölloth 2012). However, this point of $nSiO_2$ safety is controversial, and different studies reported toxic effects in some cells or organisms like humans (Brown et al. 2015; Guarnieri et al. 2014; Napierska et al. 2010), other animals (Debnath et al. 2011; Lee et al. 2009; Parveen et al. 2014), algae (van Hoecke et al. 2011) or bacteria (Adams et al. 2006). Concerning higher plants, most of the studies reported null or positive effects (Le et al. 2014; Lee et al. 2010; Lin et al. 2004; Nair et al. 2011; Siddiqui and Al-Whaibi 2014; Slomberg and Schoenfisch 2012), $nSiO_2$ toxicity being only observed at very high concentrations (Le et al. 2014; Lee et al. 2010). The toxic mechanisms of $nSiO_2$ exposure remain far from clear, but in some cases $nSiO_2$ toxic effects were related to interactions with cellular surfaces (membrane or cuticle), oxidative stress and/or

genotoxicity (Adams et al. 2006; Brown et al. 2015; Debnath et al. 2011; Fruijtier-Pölloth 2012; Napierska et al. 2010; Parveen et al. 2014).

SiO_2 nanoparticles are a common nanomaterial which is used (either or not in admixture with other elements) for a variety of applications in the medical (biomedicine, biosensor, disease labeling) and technological (food processing, ceramics synthesis, industrial and household applications) fields, but also in the environmental (wastewater treatment, water purification, environmental remediation) and agriculture fields. In agriculture, silica nanoparticles are used in different formulations, mainly as carriers in chemical delivery, or in uptake and translocation of nutrient elements, and as active ingredients against insect pests (Gogos et al. 2012), thereby fostering their dispersion in the environment. In this context, luminescent properties of CMB@SiO_2 nanoparticles are not without interest for biotechnological uses that could also be applied to plants, or to be combined with silica nanoparticles intended for agronomical uses. From these current and potential uses of silica nanoparticles, it is obvious that their potential to harm the environmental is a relevant issue. Plants, as important environmental components and sinks in terrestrial and aquatic ecosystems, are essential living organisms for testing ecological effects of nanoparticles. Hence, it is of great importance to study the impact of new functional silica nanoparticles on plant cells, and to anticipate new potential risks derived from their accumulation into plants and their subsequent fate within food chains. In earlier studies on the impact of CMB@SiO_2 nanoparticles and of CMB clusters in plant growth (Aubert et al. 2012; 2013), we showed that silica nanoparticles containing clusters have no effect on plant growth, whereas CMB clusters penetrated into roots and negatively impacted growth. In these studies, roots were always much more affected than aerial parts, certainly due to the root direct contact with clusters and the very low translocation of clusters into aerial part. The latter makes it difficult to analyze the direct impact of these nanomaterials on photosynthetic cells in these root-treated systems. Indeed, the absence of adverse effects reported in most works evaluating silica nanoparticle phytotoxicity could be partially linked to low or no occurrence of silica nanoparticles in photosynthetic cells, rather than the lack of inherent hazards. At this respect

in particular, the use of plant cell cultures provides a way for *in vitro* exposing photosynthetic cells directly to the action of nanoparticles. In fact this model system can mimic, as regards with plant cell interaction with nanoparticles, the situation that could be found in photosynthetic cells of aerial parts of plants exposed to CMB@SiO_2, nSiO_2 or CMB in a chronic way, where a higher accumulation of nanoparticles in leaves can be achieved after a long-time exposure.

In order to go further in CMB@SiO_2, nSiO_2 and CMB toxicological research, and with the aim of exploring the impact of weak doses on photosynthetic cells, we have chosen light-grown *Arabidopsis thaliana* cell suspension cultures (ACSC) as a valuable cellular system in which to investigate oxidative damage and cell response. ACSC join uniformity, homogeneity, repeatability, decoupling of cellular processes from development and slow systemic effects between cells (Menges et al. 2003), to the convenience of application of nanomaterial treatments. Here, we present studies on biochemical and oxidative stress factors on *A. thaliana* cells under exposure to functional CMB@SiO_2 nanoparticles and their components, nSiO_2 nanoparticles and CMB clusters. The in vitro cytotoxicity of these nanomaterials was examined by investigating their influence on cell growth and viability, photosynthesis, lipid peroxidation, and antioxidant enzyme activities (i.e. superoxide dismutase (SOD), guaiacol peroxidase (POD), glutathione peroxidase (GPX), glutathione reductase (GR), and glutathione S-transferase (GST) activities). Finally, the fate of nanoparticles in the medium and their penetration into plant cells was detected by transmission electron microscopy (TEM).

Materials and Methods

Chemicals, cluster units, and silica nanoparticles

Polyoxyethylene (4) lauryl ether (Brij30) and tetraethoxysilane (TEOS, 99.00%) were purchased from Sigma-Aldrich. Ammonia (28 wt % in water) and n-heptane (99.00%) were purchased from VWR. Ethanol (99.80%) was purchased from Fluka. $Cs_2Mo_6Br_{14}$ was used as the precursor of $[Mo_6Br_{14}]^{2-}$ cluster units.

Hexamolybdenum cluster units are nanometric building blocks (1 nm) constituted of a Mo_6 octahedral cluster bonded to 8 inner Br^i (i = inner) ligands capping the faces of the octahedron and 6 apical Br^a (a = apical) ligands in terminal positions. The negative charge of the $[Mo_6Br_{14}]^{2-}$ cluster unit is counter balanced by two Cs^+ cations. In solid state, the cluster units co-crystallize with the cations to form a cluster compound denoted $Cs_2Mo_6Br_{14}$. The $Cs_2Mo_6Br_{14}$ cluster compound can be dispersed as nanosized entities in ethanolic solution (Grasset et al. 2008).

All the silica nanoparticles have been prepared using a water-in-oil (W/O) microemulsion process developed by our group since the earlier 2000 (Aubert et al. 2010; Grasset et al. 2002). In this work, the complex water phase was prepared by dissolving the $Cs_2[Mo_6Br_{14}]$ cluster compound in a mixture of ethanol and distilled water (1:1 volume ratio). The concentration of the cluster sol was 0.02 M. For pure $nSiO_2$, the complex water phase was free of cluster. Finally, the nanoparticles were collected and washed by several centrifugation cycles to remove surfactant molecules before to be dispersed in purified water at concentration around 15 g L^{-1}. The average hydrodynamic size of the silica nanoparticles in water solution was estimated by dynamic light scattering (Supplementary Fig. 1) using a Malvern Zetasizer Nano ZS apparatus. All the samples were studied by TEM (Supplementary Fig. 2) using a microscope JEOL 2100 LaB_6 at 200 kV or JEOL JEM-1400 microscope operating at 120 kV. Samples for TEM analysis were prepared by placing a drop of the diluted solution in mesh copper grids, allowing the solvent in the grid to evaporate at room temperature.

ACSC growth conditions and nanomaterial treatments

The *Arabidopsis thaliana* (ecotype Col-0) cell suspension cultures were kindly provided by the Institute of Natural Resources and Agronomy from Salamanca (IRNASA-CSIC, Spain). ACSC were maintained at 24°C under sterile conditions in 200 mL of liquid growth medium (Axelos et al. 1992; Jouanneau et al. 1967) by agitation at 120 rpm and under continuous illumination (50 µE m^{-2} s^{-1}) in an incubator shaker (Innova 42R, NBS). For nanoparticle toxicity tests, we applied luminescent silica nanoparticles (CMB@SiO_2) and their constituents (i.e. CMB clusters and nSiO_2) into 9 days-old ACSC (cell density of 150-200 mg mL^{-1}). For these studies, three different concentrations of CMB@SiO_2 and nSiO_2 (1, 10 and 100 mg L^{-1}), and of CMB clusters (1, 7.5 and 60 mg L^{-1}) were tested. Treated ACSC were incubated for up to three days under normal growth conditions, and sample aliquots collected at 3, 24 and 72 h. Collected samples were centrifuged at 4000 rpm for 5 min, the supernatant was removed, and the cell pellet was weighed, frozen in liquid nitrogen and finally stored at -80°C until further analysis.

For stock solutions to be used for nanoparticle toxicity tests, CMB@SiO_2 and nSiO_2 were suspended in water at 5 g L^{-1}, and CMB in 50% ethanol at 60 g L^{-1}. CMB@SiO_2 used here are composed of 7.5% clusters and 92.5% SiO_2 (Aubert et al. 2013). Thus, the intermediate CMB concentration (7.5 mg L^{-1}) used for treatments corresponds to the cluster content associated to the intermediate concentration of CMB@SiO_2 nanoparticles (100 mg L^{-1}). From this intermediate CMB concentration, we have set the lowest CMB concentration at 1 mg/L, which correspond (rounded to the nearest unit) to the cluster content present in 10 mg/L of CMB@SiO_2, and the highest CMB concentration at 60 mg/L (in order not to exceed 0.05% of ethanol in cell culture medium). As control, we used ACSC without added nanomaterial but containing the equivalent volume of the corresponding solvent or medium as used for the nanomaterial tested.

Cell viability assay

Cell mitochondria and metabolic activities were measured by the MTT (3-(4,5-dimethylthiazol-2-yl)-2,5-diphenyl tetrazolium bromide) test following manufacturer's indications (Cell growth determination kit CGD-1, Sigma-Aldrich). Cell density was adjusted to 25 mg mL^{-1} at the beginning of the treatment, and cell dilution for MTT assay was the same for all the samples. Relative cell viability was expressed as the percentage of control untreated cells and calculated by $[\text{Absorbance}_{570\,nm} - \text{Absorbance}_{690\,nm}]_{test} / [A_{570} - A_{690}]_{control} \times 100$.

Pigment analysis

The chlorophyll and carotenoid contents were determined spectrophotometrically following Lichtenthaler and Wellburn (1983) equations. Collected cells were lyophilised (Christ ALPHA 1-2LDplus) and pigments extracted from 20 mg dry weight (DW) by overnight pure acetone extraction at 4°C. The absorbance was quantified at 470, 645 and 663 nm using a micro plate spectrophotometer (SAFAS, Xenius).

Chlorophyll fluorescence measurements

Modulated chlorophyll fluorescence measurements were made in ACSC (previously dark adapted for 30 min) with a PAM-210 chlorophyll fluorometer (Heinz Walz). Maximum quantum yield of photosynthesis was estimated by the F_v/F_m ratio from dark-adapted ACSC, where F_v is calculated subtracting the minimal fluorescence (F_o) to the maximal fluorescence (F_m).

Lipid peroxidation

The level of lipid peroxidation was determined by measuring the amount of TBARS (thiobarbituric acid reactant species) produced by the thiobarbituric acid (TBA) reaction, according to the corrected TBA method as described by Hodges et al. (1999) adapted to 96-well plates.

Antioxidant enzyme extraction and activity assays

Enzyme extracts correspond to supernatants obtained after homogenizing *A. thaliana* cells in sodium phosphate buffer (50 mM, pH 7.5) with Na-EDTA (1 mM), polyvinyl-pyrrolidone (5 % w/v), sodium ascorbate (5 mM) and Protease Inhibitor Cocktail (0.5 % v/v, Sigma-P9599) at a ratio of 1 mL per 20 mg DW. Protein contents were determined according to Bradford (Bradford 1976), using bovine serum albumin as the standard protein. Enzyme extracts were frozen in liquid nitrogen and kept at -80°C until their use for enzymatic assays. All enzyme assays were adapted to 96-well plates (final reaction volume of 300 µL).

SOD activity was determined based on the inhibition of the reduction of nitro-blue tetrazolium (NBT) into formazan in the presence of riboflavin as described by Giannopolitis and Ries (1977). Formazan formation was determined measuring the absorbance at 560 nm after 10 min of incubation under white light at 25 ºC. The reaction mixture consisted of 10 µL of enzyme extract, potassium phosphate buffer (50 mM, pH 7.8), EDTA (0.1 mM), NBT (75 µM), methionine (13 mM) and riboflavin (2 µM).

POD activity was measured by the method of Srivastava and van Huystee (1977) with a reaction mixture consisting of 5 µL of enzyme extract, potassium phosphate buffer (100 mM, pH 6.5), H_2O_2 (0.05% v/v) and guaiacol (15 mM). The enzymatic activity was determined from the maximum rate of tetragaiacol formation by monitoring the increase in absorbance at 470 nm ($\varepsilon_{Tetragaiacol}$ = 26.6 mM^{-1} cm^{-1}).

GPX activity was measured by a coupled assay system in which oxidation of GSH was coupled to NADPH oxidation catalyzed by glutathione reductase according to the method of Floh and

Günzler (1984). The reaction mixture consisted of 5 µL of enzyme extract, potassium phosphate buffer (100 mM, pH 7.0), cumene hydroperoxide (0.5 mM), GSH (4 mM), NADPH (0.2 mM) and 0.5 units of yeast glutathione reductase. The enzymatic activity was determined at 25ºC from the maximum rate of NADPH oxidation by monitoring the decrease in absorbance at 340 nm (ε_{NADPH} = 6.22 mM^{-1} cm^{-1}).

GR activity was measured according to the method of Carlberg and Mannervik (1985), following the oxidized glutathione (GSSG)-dependent oxidation of NADPH. The assay mixture consisted of 10 µL of enzyme extract, HEPES buffer (50 mM, pH 8.0), EDTA (0.5 mM), GSSG (0.5 mM) and NADPH (0.25 mM). The enzymatic activity was determined at 25ºC from the maximum rate of NADPH oxidation by monitoring the decrease in absorbance at 340 nm (ε_{NADPH} = 6.22 mM^{-1} cm^{-1}).

GST activity was measured by the method of Habig and Jacoby (1981) using CDNB (l-chloro-2, 4-dinitrobenzene) as the substrate. The assay mixture consisted of 5 µL of enzyme extract, potassium phosphate buffer (100 mM, pH 7.4), GSH (1 mM) and CNDB (1 mM). The enzymatic activity was determined at 25ºC from the maximum rate of GSH/CNDB conjugate formation by monitoring its absorbance at 340 nm (ε_{CNDB} = 9.6 mM^{-1} cm^{-1}).

All enzymatic activities but SOD were expressed as nkat mg^{-1} protein. SOD activity was expressed as U mg^{-1} protein, U (a unit) being the amount of enzyme causing 50% inhibition of the NBT reduction observed in the absence of enzyme.

ACSC TEM analysis

TEM samples were prepared following standard procedures. Roughly, collected cell samples were centrifuged at 1700 *g* for 5 min, the supernatants were removed, and the cell pellets were washed once with cacodylate buffer, chemically prefixed in 2.5 % (v/v) glutaraldehyde for 1.5 h, washed 3 times in sodium cacodylate buffer (0.2 M, pH 7.1), then post fixed in 0.5 % (v/v) osmium tetroxide for 1 h, and washed 3 times in sodium cacodylate buffer (0.2 M, pH 7.1). The samples were then

included in low melting agar (4%) and dehydrated in several ethanol baths with increasing concentrations. The specimens were embedded in an Araldite/Epon epoxy resin from which ultrathin sections (thickness: 90 nm) were cut using an ultramicrotome (LEICA UC7) and directly deposited on copper grids. The grids were visualized in a JEOL 1400 microscope operated at 120 kv and using a Gatan 2kX2k Orius camera. Image analysis on the silica nanoparticles and clusters was carried out on 35 TEM images. The processing of the image files was performed on more than 500 particles using standard ImageJ analysis software (http://rsbweb.nih.gov/ij/). Particle size is presented as mean ± standard deviation (SD).

Statistical analysis

Statistical analyses were performed with R software version 3.2.1 (http://www.r-project.org/). Normality and homoscedasticity were confirmed with Shapiro and Bartlett tests for each assay. The results are presented as mean ± standard error of the mean (SEM) of three independent experiments. Differences between means were evaluated for significance by Student's t-test for pairwise comparisons, and by one-way analysis of variance (ANOVA) followed of Tukey's test for multiple comparisons. Statistical significance was accepted when $p < 0.05$.

Results

Particle characterization

The hydrodynamic diameter of the two types of silica nanoparticles was found to be comprised between 40-60 nm from the dynamic light scattering data in aqueous dispersion at pH = 7.4, which indicates that the nanoparticles are not or slightly aggregated in the solution. The result obtained for

CMB@SiO_2 is represented in Supplementary Fig. 1 as example. These results are in the same range as the size observed by scanning electron microscopy (not shown) and TEM. The TEM images of the $nSiO_2$ and CMB@SiO_2 are as shown in Supplementary Fig. 2. Diameter sizes of 'as produced' CMB@SiO_2 and $nSiO_2$ obtained from the TEM image are of 47 ± 3 and 29 ± 2 nm, respectively.

Impacts of nanomaterials on cell growth and cell viability

In our conditions, ACSC grew with a doubling time of about 2.1 days and had a cell density around 200 mg mL^{-1} at the beginning of the stationary phase (between 9 to 11 days after subculture). No changes in cell growth or viability were observed 3 h after exposure, regardless of nanomaterial (Fig. 1a-c). However, depending on the type of nanomaterial, significant changes in cell growth were detected during longer treatment periods. Thus, while ACSC exposed to CMB@SiO_2 or $nSiO_2$ at concentrations up to 100 mg L^{-1} are capable to continue normal growth up to 72 h after treatment (Fig. 1a, b), 60 mg L^{-1} CMB significantly impacted ACSC growth (18.5 and 21.3 % of growth inhibition after 24 and 72 h of treatment, respectively) (Fig. 1c).

On the other hand, *Arabidopsis* cell viability was assessed by the MTT assay (Fig. 1d-f). In agreement with the impact of nanomaterials on cell growth, only CMB clusters at their highest used concentration had significant cytotoxic effects, provoking a 45.6 and 27.7 % decrease of cell viability after 24 and 72 h of exposure respectively (Fig. 1f).

Changes in chloroplast pigment content and photosynthetic efficiency

The impact of nanomaterials on chloroplasts was evaluated through the analyses of chlorophyll and carotenoid contents, and PSII photochemical efficiency. Light-grown ACSC used for nanomaterial treatments were pale green and contained about 240 µg chlorophyll and 85 µg carotenoid per gram DW. Chlorophyll content remained unchanged during treatment in light-grown control, and in

CMB@SiO_2 and nSiO_2 treated ACSC, whereas ACSC treated with 60 ppm CMB experienced a 13 and 21% decline in chlorophyll content after 24 and 72 h of treatment respectively (Fig. 2a–c). Concerning carotenoid content, we roughly observed a similar behavior as for chlorophyll, CMB clusters being the only nanomaterial to have a significant impact on it (Fig. 2d–f). Finally, it should also be noted that the chlorophyll a/b and chlorophyll/carotenoid mass ratios in control ACSC at the beginning of the treatment were approximately 3.7 and 2.7 respectively, and that they were not affected by any of the nanomaterials (data not shown).

The maximum quantum yield of photosynthesis is generally influenced by stress situations, and is usually estimated by the ratio Fv/Fm. The maximum quantum yield of photosynthesis in light-grown ACSC reached a level of around 0.45-0.55 in 9-days-old ACSC used for nanomaterial treatments, and changed little during treatment time course. CMB@SiO_2 treatments did not affected F_v/F_m values (Fig. 2g, h) but CMB significantly did (Fig. 2i) through 24-72 hours of treatment at all the tested concentrations.

Oxidative impact and enzymatic antioxidant response

We studied the mechanisms of cytotoxicity caused by nanomaterials with respect to oxidative stress through the oxidative impact on lipids (lipid peroxidation) and the antioxidant response (antioxidant enzymatic activities). The oxidative degradation of lipids by reactive oxygen species (ROS), called lipid peroxidation, results in the formation of highly reactive and unstable lipid peroxides which decomposed into TBARS, including malondialdehyde (MDA). Thus, TBARS level give a convenient estimation of the relative lipid peroxide content. The TBARS content of control 9-day-old ACSC was ≈14-16 nmol $MDA_{equivalents}$ g^{-1}. After nanomaterial exposure, a significant increase of lipid peroxidation was only observed for 60 mg L^{-1} CMB-treated cells (Fig. 3). In this case, lipid peroxidation increased with time treatment, being of 119% after 24 h and 143% after 72 h of treatment.

In order to understand the adaptability and to determine the nature of the antioxidant responses of *A. thaliana* cells to the different nanomaterials, we analyzed the activities of five antioxidant enzymes, i.e. superoxide dismutase (SOD; EC 1.15.1.1), guaiacol peroxidase (POD; EC 1.11.1.7), glutathione peroxidase (GPX; EC 1.11.1.9), glutathione reductase (GR; EC 1.8.1.7) and glutathione S-transferase (GST; EC 2.5.1.18), in ACSC treated for 3, 24 and 72 hours with investigated nanoparticles at different concentrations. The only nanomaterial affecting SOD (Fig. 4a–c), POD (Fig. 4d–f) and GR (Fig. 4g–i) activities were CMB clusters. Thus, *A. thaliana* cells undergoing 60 ppm CMB treatment showed, relative to control, a 50% transitory increase in SOD activity after 24 h, and a marked increase in POD (2 and 1.9 times) and GR (1.6 and 1.5 times) activities after 24 and 72 h of treatment. On the other hand, GPX activity (Fig. 4j–l) was increased by all the nanomaterials tested, but with different induction patterns. Thus, while 60 ppm CMB clusters induced GPX after 24 and 72 h of treatment, CMB@SiO_2 and nSiO_2 slightly induced GPX after 3 h, and nSiO_2 was able to provoke a second wave of inductions in a concentration-dependent way after 72 h. Finally, concerning GST activity (Fig. 4m–o), all the nanomaterials at the different concentrations were able to early induce GST (3 h after treatment). The highest increase of GST activity was obtained after nSiO_2 treatment, but only 60 ppm CMB maintained GST induction over time.

Nanoparticle interaction with plant cells as examined by TEM

In culture medium (‘as exposed’ state), CMB clusters showed tendency to aggregate forming particles of a diameter around 83 ± 14 nm, which agglomerate to form different shape branched structures under the micrometer range (Fig. 5a). On the other hand, ‘as exposed’ CMB@SiO_2 and nSiO_2 stayed non aggregated and spherical in shape with diameters, as measured from TEM micrographs, of 44 ± 4 and 27 ± 2 nm, respectively (Fig. 5b, c). These nanoparticle sizes were not

significantly different from ‘as produced’ sizes measured from TEM micrographs (Supplementary Fig. 2).

In addition, *Arabidopsis* cells were also observed by TEM to determine if the different nanomaterials entered the plant cells. In the case of CMB treated cells (Fig. 5a, d), they display altered cell wall ultrastructure, presenting a loosely structured cell wall (reduced electron density) but more than twice as thick compared with that of control cells (Supplementary Fig. 3). Cluster aggregates seem to be present inside this loose cell wall and central vacuole, but are not observed inside vesicles. Furthermore, we cannot rule out the presence of individual nanometric clusters which, as already mentioned, are not detectable when they are at their synthesis size (1 nm diameter) due to resolution limit of the TEM available for this work. In contrast, CMB@SiO_2 (Fig. 5b, e) and nSiO_2 (Fig. 5c, f) were observed inside plant cells and seemed to conserve their ‘as produced’ and ‘as exposed’ sizes. Furthermore, CMB@SiO_2 and nSiO_2 were observed inside vesicles (Fig. 5d, e), pointing endocytosis as a mechanism of cell uptake for these nanoparticles.

Discussion

Luminescent functional silica nanoparticles based on Mo_6 clusters possess a huge potential for application in the field of nanobiotechnology or nanophotonics (Cordier et al. 2015). For a reasonable and responsible development of their use, potential toxic effects must be deeply studied. Here, the cytotoxicity of low/medium doses of functional silica nanoparticles and their components was investigated under *in vitro* conditions using photosynthetic *A. thaliana* cell cultures. CMB clusters at 60 ppm concentration negatively impacted cells, significantly reducing cell growth and viability (Fig. 1) in agreement with their reported negative impact on plant root growth (Aubert et al. 2012). In the case of silica nanoparticles, none negative effect were observed on ACSC growth or viability after neither CMB@SiO_2 nor ‘empty’ nSiO_2 treatments at any tested concentration.

384 Slomberg and Schoenfisch (2012) already showed that $nSiO_2$ did not caused toxic effects on *A.*
385 *thaliana* plants up to 1 g L^{-1}, but in this case $nSiO_2$ contact with photosynthetic cells was negligible
386 since they reported minimal upward translocation to foliage.

387 The impact of $CMB@SiO_2$, $nSiO_2$ and CMB on chloroplast functioning has never been
388 evaluated. We have first showed that although photosynthesis is not necessary for ACSC survival,
389 the photosynthetic electron transport chain of thylakoid membranes in light-grown ACSC is active
390 (Fig. 2). Thus, we measured quantum yield of photosynthesis (F_v/F_m) values around 0.6 for control
391 ACSC, which is in agreement with those from the literature for *A. thaliana* cell cultures (González-
392 Pérez et al. 2011) and indicates that *A. thaliana* cell cultures produce functional chloroplasts, even if
393 this ratio is lower than the 0.8 determined for green leaves (Zhang et al. 2008). In addition, the
394 levels of chlorophylls (240 µg g^{-1} DW) and carotenoids (85 µg g^{-1} DW) were in perfect agreement
395 with those described in the literature for *A. thaliana* cell cultures (González-Pérez et al. 2011; Doyle
396 et al. 2010) and represent, respectively, about 2.5% and 5.5 % of the levels described in leaf tissues
397 (Zhang et al. 2008; Doyle et al. 2010). Furthermore, while the chlorophyll *a*/*b* ratio (around 3.7)
398 was close to those for mature chloroplasts of *A. thaliana* leaves (around 3.3), the
399 chlorophyll/carotenoid mass ratio (around 2.7) was much lower than in *A. thaliana* leaves (around
400 6.4) (Zhang et al. 2008). Photosynthetic apparatus parameters such as pigment content (chlorophylls
401 and carotenoids), pigment ratios, and photosynthesis yield are good indicators for stress detection
402 and tolerance (Doyle et al. 2010; Zhang et al. 2008). In our work, only CMB clusters significantly
403 impacted these parameters, decreasing chlorophyll and carotenoid contents as well as F_v/F_m values,
404 but without affecting Chl *a*/*b* or chlorophyll/carotenoid ratios. It is worth to be noted that a
405 significant decreased in maximum quantum yield of photosynthesis was observed for CMB doses as
406 low as 1 ppm. This photosynthetic unbalance can generate excess energy, which is extremely
407 harmful and dangerous for plant cell metabolism, notably because it provokes the accumulation of
408 ROS which may lead to damages in the thylakoid membranes and protein modulation (Ruban
409 2015). In the light of the foregoing, photosynthetic apparatus seems to be more sensitive to CMB

under light conditions than cell growth or viability. This can be attributed to the fact that light enhances ROS production by clusters, precisely $^1O_2$ (Aubert et al. 2013), and that this could synergically interact with ROS production in different organelles, notably those associated to photosynthetic light-driven process: $^1O_2$ in PSII, superoxide radical ($O_2^{\cdot -}$) in PSI, and hydrogen peroxide (H_2O_2) in the chloroplast stroma (Gill and Tuteja 2010).

We have shown in previous work that $^1O_2$ production involving CMB clusters can be prevented, to some extent, by the encapsulation of the cluster units in silica nanoparticles (Aubert et al. 2013). However, the capacity of CMB to provoke an oxidative stress in cells, and the impact of silica encapsulation on this, has never been studied. It is well known that the generation of ROS as natural by-products during cell metabolism is enhanced in the different plant cell compartments after the exposure of plants to environmental stresses, provoking subsequent damage in cell biomolecules and metabolism. We chose to follow MDA production (through TBARS quantification) because MDA is a product of the peroxidation of unsaturated fatty acids and it has been used as an indicator of free radical damage to cell membranes under stress conditions (Gill and Tuteja 2010). Under nanomaterial treatment, the TBARS content was found to be increased only after CMB cluster exposure. This could be explained on the basis of the above mentioned $^1O_2$ production by CMB under light conditions, as it has been shown that $^1O_2$ mediate lipid peroxidation (Triantaphylidès et al. 2008), and matches with previous studies showing that the CMB@SiO_2 nanoparticles are particularly stable and do not liberate clusters (Aubert et al. 2013). Furthermore, even if oxygen has been shown to still have access to some cluster units from CMB@SiO_2 and produce $^1O_2$, we showed here that silica encapsulation of CMB clusters prevents $^1O_2$ production at levels able to provoke lipid peroxidation in *A. thaliana* cells.

To protect themselves against ROS production and uncontrolled lipid peroxidation, plant cells possess and induce an array of antioxidant defense systems (Gill and Tuteja 2010). We analyzed the activities of an array of antioxidant enzymes (SOD, POD, GPX, GR and GST) under nanomaterial treatment conditions. Within these activities, SOD, which catalyze disproportionation of $O_2^{\cdot -}$ into

436 H_2O_2 and O_2, belong to the first line of defense. The H_2O_2 produced in the cell, by SOD or other
437 processes, may be scavenged by catalases and peroxidases, the latter including POD and GPX.
438 Additionally, GPX may also reduce lipid hydroperoxides. For their part, GST catalyze the
439 conjugation of electrophilic substrates to reduced glutathione, and can also function as glutathione
440 peroxidases. Finally, the glutathione oxidized in cells is regenerated by GR utilizing NADPH. The
441 increment in the activity of SOD after 24 h of exposure to CMB, and the higher increase of POD
442 and GR activities after CMB treatment at 24 and 72 h, suggested their role in the defense system
443 against CMB induced oxidative stress, either by the removal of ROS and of toxic products of
444 organic peroxidation. Moreover, the induction of POD, which are mainly considered extracellular
445 proteins, in interplay with apoplastic SOD could participate in initial oxidative burst and signal
446 transduction pathways (Francoz et al. 2015) as well as cell wall loosening (Minibayeva et al. 2015).
447 Interestingly, the latter have been observed in CMB treated cells (Fig. 5 and Supplementary Fig. 3).
448 It should also be pointed out that, in agreement with the absence of physiological (cell growth and
449 viability, pigments, and quantum yield of photosynthesis) and oxidative (lipid peroxidation)
450 impacts, CMB@SiO_2 and nSiO_2 treatments did not have a marked impact on antioxidant activities,
451 exception done of the induction of GR activity by nSiO_2 after a long exposure period (72 h), and the
452 early induction of GST activity by both silica nanoparticles.

453 It is well-known that the properties of nanomaterials can change from the form in which they are
454 synthesized to the form to which biological test systems are exposed, and that these potential
455 changes in size, shape or aggregation, among other, could influence toxicity. In previous studies we
456 showed that the CMB clusters and cluster aggregates can be found in a wide range of sizes
457 depending on the dispersing medium, and that their concentration-dependent toxicity depends on
458 their aggregation state (Aubert et al. 2012). Consequently, here we analyzed using TEM the
459 different nanomaterials in the exposure medium and in intimate contact with living cells. Even if
460 silica nanoparticles can have tendency to agglomerate and aggregate in high ionic strength medium
461 like growth medium (Guarnieri et al. 2014), we observed that hydrophilic CMB@SiO_2 and nSiO_2

462 do not aggregate in plant cell growth medium and presented similar size and shape that 'as
463 produced' (Fig. 5b, c). It should be mentioned that due to the resolution limit of the TEM available
464 for this work, it is not possible to see the nanosized metal cluster inside the CMB@SiO_2 silica
465 nanoparticles. For this particular point, the reader should see Grasset et al. (2008). In contrast, as
466 expected from our previous work, 1 nm CMB clusters aggregate forming structures with "spheric-
467 like" shapes that further agglomerates into ramified structures of different shapes and sizes (Fig.
468 5a). Actually, even if cluster units are nanosized entities, they are hydrolyzed in presence of water
469 and co-precipitate with water molecules to form the crystalline compound
470 $[(Mo_6Br^i_8)(OH)^a_4(H2O)^a_2]\bullet 12H_2O$. However, it is worth to be noted that the sizes of aggregates (up
471 to one hundred nanometers) in present work conditions were smaller than in previous ones (from
472 several hundred nanometers to few micrometers), and that shapes are also different to the disc-like
473 aggregates previously observed. The TEM grid preparation could be one reason to explain this
474 difference.

475 The uptake and bioaccumulation of nanoparticles by plants is crucial in many respects, such as
476 environmental issues, food-chain transfer, biotechnological applications and interaction with cell
477 organelles or toxicity. There have been only a few studies examining silica nanoparticle uptake by
478 plants. These studies reported different degrees of nanoparticle root uptake and internalization onto
479 plant cells, and more rarely their upward translocation into shoots (Le et al. 2014; Nair et al. 2011;
480 Slomberg and Schoenfisch 2012; Torney et al. 2007; Vivero-Escoto et al. 2012). In our system, we
481 observed that both silica nanoparticles intimately interact with the cell wall, and seem to be
482 internalized into *Arabidopsis* cells by endocytosis since they were mainly found encapsulated in
483 vesicles (Fig. 5e, f). Indeed, recent studies have shown that plant cells are able to accomplish
484 endocytosis for the internalization of molecules from the extracellular environment in a process
485 resembling mammalian cell endocytosis (Fan et al. 2015). In contrast, CMB clusters were observed
486 forming aggregates inside cell walls and vacuoles, but not inside vesicles, suggesting that clusters

mainly penetrate by passive diffusion as nanosized entities. We already described this situation in root cells of *A. thaliana* seedlings treated with CMB (Aubert et al. 2012).

A final consideration concerns the potential participation of ion release in the toxicity of the evaluated nanomaterials. The observed perturbation of cell growth and metabolism in response to Mo-based clusters cannot be ascribed to the eventual release of metal ions as we already showed that only the apical Br ligands (6 atoms) and the Cs counter cations (2 atoms) were liberated from clusters in culture medium, but no Mo was released in the solution as ionic species. At the highest concentration of CMB clusters (60 mg L^{-1} = 0.0306 mM) used in the present study, levels of Cs^+ and Br^- ions liberated would be 0.0612 and 0.1836 mM respectively, which is far down toxic concentrations for these ions (Aubert et al. 2012).

Conclusion

ACSC showed to be an appropriate screening system to assess plant biological responses to nanomaterials, allowing proper interactions of the biological system with the evaluated nanomaterials. We showed in this study that Mo_6-based clusters, even at low doses, present a significant toxicity for plant cells, negatively affecting growth, viability and photosynthesis, and increasing oxidative impact, which provoked stimulation of antioxidant enzymatic activities. Based on the results presented here, it is also concluded that the encapsulation of the clusters into silica, which showed to be biologically compatible in our conditions, protected the plant cells by avoiding direct contact of harmful clusters with cellular structures and the generation of oxidative stress. Thus, deleterious impacts were not observed after CMB@SiO_2 nanoparticle exposure, and nSiO_2 nanoparticles neither showed cytotoxic effects, despite intimate contact with cells and their internalization.

513

514 **References**

515

516 Adams LK, Lyon DY, Alvarez PJJ (2006) Comparative eco-toxicity of nanoscale TiO_2, SiO_2, and
517 ZnO water suspensions. Water Res 40:3527–3532. doi:10.1016/j.watres.2006.08.004

518 Aubert T, Burel A, Esnault M-A, Cordier S, Grasset F, Cabello-Hurtado F (2012) Root uptake and
519 phytotoxicity of nanosized molybdenum octahedral clusters. J Hazard Mater 219-220:111−118.
520 doi:10.1016/j.jhazmat.2012.03.058

521 Aubert T, Cabello-Hurtado F, Esnault M-A, Neaime C, Lebret-Chauvel D, Jeanne S, Pellen P,
522 Roiland C, Le Polles L, Saito N, Kimoto K, Haneda H, Ohashi N, Grasset F, Cordier S (2013)
523 Extended investigations on luminescent $Cs_2[Mo_6Br_{14}]@SiO_2$ nanoparticles: physico-structural
524 characterizations and toxicity studies. J Phys Chem C 117:20154–20163.
525 doi:10.1021/jp405836q

526 Aubert T, Grasset F, Mornet S, Duguet E, Cador O, Cordier S, Molard Y, Demange V, Mortier M,
527 Haneda H (2010) Functional silica nanoparticles synthesized by water-in-oil microemulsion
528 processes. J Colloid Interface Sci 341:201–208. doi:10.1016/j.jcis.2009.09.064

529 Axelos M, Curie C, Mazzolini L, Bardet C, Lescure B (1992) A protocol for transient gene
530 expression in *Arabidopsis thaliana* protoplasts isolated from cell suspension cultures. Plant
531 Physiol Biochem 30:123–128.

532 Baker GL, Ghosh RN, Osborn DJ (2010) Sol–gel encapsulated hexanuclear clusters for oxygen
533 sensing by optical techniques. U.S. Patent 7,858,380

534 Bradford MM (1976) A rapid and sensitive method for the quantitation of microgram quantities of
535 protein utilizing the principle of protein-dye binding. Anal Biochem 72:248–54

536 Buzea C, Pacheco II, Robbie K (2007) Nanomaterials and nanoparticles: sources and toxicity.
537 Biointerphases 2:MR17–MR71. doi:10.1116/1.2815690

538 Brown DM, Varet J, Johnston H, Chrystie A, Stone V (2015) Silica nanoparticles and biological

539 dispersants: genotoxic effects on A549 lung epithelial cells. J Nanopart Res 17:1–16.
540 doi:10.1007/s11051-015-3210-3
541 Carlberg I, Mannervik B (1985) Glutathione reductase. Methods Enzymol 113:484–490.
542 Colvin V-L (2003) The potential environmental impact of engineered nanomaterials. Nat
543 Biotechnol 21:1166–1170. doi:10.1038/nbt875
544 Cordier S, Grasset F, Molard Y, Amela-Cortes M, Boukherroub R, Ravaine S, Mortier M, Ohashi
545 N, Saito N, Haneda H (2015) Inorganic molybdenum octahedral nanoclusters, versatile
546 functionnal building block for nanoarchitectonics. J Inorg Organomet Polym Mater 25:189–
547 204. doi:10.1007/s10904-014-0112-2
548 Debnath N, Das S, Chandra DSR, Bhattacharya SCh, Goswami A (2011) Entomotoxic effect of
549 silica nanoparticles against *Sitophilus oryzae* (L.). J Pest Sci 84:99–105. doi:10.1007/s10340-
550 010-0332-3
551 Doyle SM, Diamond M, McCabe PF (2010) Chloroplast and reactive oxygen species involvement
552 in apoptotic-like programmed cell death in *Arabidopsis* suspension cultures. J Exp Bot 61:473–
553 482. doi:10.1093/jxb/erp320
554 Fan L, Li R, Pan J, Ding Z, Lin J (2015) Endocytosis and its regulation in plants. Trends Plant Sci
555 20:388–397. doi:10.1016/j.tplants.2015.03.014
556 Floh L, Günzler WA (1984) Assays of glutathione peroxidase. Methods Enzymol 105:114–121
557 Francoz E, Ranocha P, Nguyen-Kim H, Jamet E, Burlat V, Dunand C (2015) Roles of cell wall
558 peroxidases in plant development. Phytochem 112:15–21.
559 doi:10.1016/j.phytochem.2014.07.020
560 Fruijtier-Pölloth C (2012) The toxicological mode of action and the safety of synthetic amorphous
561 silica-A nanostructured material. Toxicology 294:61–79. doi:10.1016/j.tox.2012.02.001
562 Giannopolitis CN, Ries SK (1977) Superoxide dismutase I. Occurrence in higher plants. Plant
563 Physiol 59:309–314.
564 Gill SS, Tuteja N (2010) Reactive oxygen species and antioxidant machinery in abiotic stress

565 tolerance in crop plants. Plant Physiol Biochem 48:909–930. doi:10.1016/j.plaphy.2010.08.016
566 Gogos A, Knauer K, Bucheli TD (2012) Nanomaterials in plant protection and fertilization: current
567 state, foreseen applications, and research priorities. J Agr Food Chem 60:9781−9792.
568 doi:10.1021/jf302154y
569 González-Pérez S, Gutiérrez J, García-García F, Osuna D, Dopazo J, Lorenzo O, Revuelta JL,
570 Arellano JB (2011) Early transcriptional defense responses in *Arabidopsis* cell suspension
571 culture under high-light conditions. Plant Physiol 156:1439–1456. doi/10.1104/pp.111.177766
572 Guarnieri D, Malvindi MA, Belli V, Pompa PP, Netti P (2014) Effect of silica nanoparticles with
573 variable size and surface functionalization on human endothelial cell viability and angiogenic
574 activity. J Nanopart Res 16:1–14. doi:10.1007/s11051-013-2229-6
575 Grasset F, Dorson F, Cordier S, Molard Y, Perrin C, Marie AM, Sasaki T, Haneda H, Bando Y,
576 Mortier M (2008) Water-in-oil microemulsion preparation and characterization of
577 $Cs_2Mo_6X_{14}@SiO_2$ phosphor nanoparticles based on transition metal clusters (X = Cl, Br, and I).
578 Adv Mater 20:143–148. doi:10.1002/adma.200701686
579 Grasset F, Labhsetwar N, Li D, Park DC, Saito N, Haneda H, Cador O, Roisnel T, Mornet S,
580 Duguet E, Portier J, Etourneau J (2002) Synthesis and magnetic characterization of zinc ferrite
581 nanoparticles with different environments: powder, colloidal solution and zinc ferrite-silica
582 core-shell nanoparticles. Langmuir 18:8209–8216. doi:10.1021/la020322b
583 Habig WH, Jakoby WB (1981) Assays for differentiation of glutathione-S-transferases. Methods
584 Enzymol 77:398–405
585 Hodges DM, DeLong JM, Forney CF, Prange RK (1999) Improving the thiobarbituric acid-
586 reactive-substances assay for estimating lipid peroxidation in plant tissues containing
587 anthocyanin and other interfering compounds. Planta 207:604–611. doi:
588 10.1007/s004250050524
589 Jouanneau JP, Péaud-Lenoël C (1967) Growth and synthesis of proteins in cell suspensions of a
590 kinetin dependent tobacco. Physiol Plant 20:834–850

591 Le V, Rui Y, Gui X, Li X, Liu S, Han Y (2014) Uptake, transport, distribution and Bio-effects of
592 SiO_2 nanoparticles in Bt-transgenic cotton. J Nanobiotechnology 12:50. doi:10.1186/s12951-
593 014-0050-8
594 Lee CW, Mahendra S, Zodrow K, Li D, Tsai YC, Braam J, Alvarez PJ (2010) Developmental
595 phytotoxicity of metal oxide nanoparticles to *Arabidopsis thaliana*. Environ Toxicol Chem
596 29:669-675. doi:10.1002/etc.58
597 Lee SW, Kim SM, Choi J (2009) Genotoxicity and ecotoxicity assays using the freshwater
598 crustacean *Daphnia magna* and the larva of the aquatic midge *Chironomus riparius* to screen
599 the ecological risks of nanoparticle exposure. Environ Toxicol Phar 28:86–91.
600 doi:10.1016/j.etap.2009.03.001
601 Lichtenthaler HK, Wellburn AR (1983) Determination of total carotenoids and chlorophyll *a* and *b*
602 of leaf extract in different solvents. Biochem Soc T 11:591–592
603 Lin BS, Diao SQ, Li CH, Fang LJ, Qiao SC, Yu M (2004) Effect of TMS (nanostructured silicon
604 dioxide) on growth of Changbai larch seedlings. J For Res-CHN 15:138–140. doi:
605 10.1007/BF02856749
606 Long JR, Xheng X, Holm RH, Yu S-B, Droege M, Sanderson WA (1998) Contrast agents. U.S.
607 Patent 5,804,161
608 Menges M, Hennig L, Gruissem W, Murray JAH (2003) Genome-wide gene expression in an
609 *Arabidopsis* cell suspension. Plant Mol Biol 53:423–442. doi:
610 10.1023/B:PLAN.0000019059.56489.ca
611 Minibayeva F, Beckett RP, Ilse K (2015) Roles of apoplastic peroxidases in plant response to
612 wounding. Phytochem 112:122–129. doi:10.1016/j.phytochem.2014.06.008
613 Nair R, Poulose A, Nagaoka Y, Yoshida Y, Maekawa T, Kumar DS (2011) Uptake of FITC labeled
614 silica nanoparticles and quantum dots by rice seedlings: effects on seed germination and their
615 potential as biolabels for plants. J Fluoresc 21:2057–2068. doi:10.1007/s10895-011-0904-5
616 Napierska D, Thomassen LC, Lison D, Martens JA, Hoet PH (2010) The nanosilica hazard: another

variable entity. Part Fibre Toxicol 7:39. doi:10.1186/1743-8977-7-39

Parveen A, Rizvi SHM, Mahdi F, Tripathi S, Ahmad I, Shukla RK, Khanna VK, Singh R, Patel DK, Mahdi AA (2014) Silica nanoparticles mediated neuronal cell death in corpus striatum of rat brain: implication of mitochondrial, endoplasmic reticulum and oxidative stress. J Nanopart Res 16:1–15. doi:10.1007/s11051-014-2664-z

Ruban AV (2015) Evolution under the sun: optimizing light harvesting in photosynthesis. J Exp Bot 66: 7–23. doi:10.1093/jxb/eru400

Selvan ST, Tan TT, Yi DK, Jana NR (2010) Functional and multifunctional nanoparticles for bioimaging and biosensing. Langmuir 26:11631–11641. doi:10.1021/la903512m

Siddiqui MH, Al-Whaibi MH (2014) Role of nano-SiO_2 in germination of tomato (*Lycopersicum esculentum* seeds Mill.). Saudi J Biol Sci 21:13–17. doi:10.1016/j.sjbs.2013.04.005

Slomberg DL, Schoenfisch MH (2012) Silica nanoparticle phytotoxicity to *Arabidopsis thaliana*. Environ Sci Technol 46:10247−10254. doi:10.1021/es300949f

Srivastava OP, van Huystee RB (1977) IAA oxidase and polyphenol oxidase activities of peanut peroxidase isoenzymes. Phytochem 16:1527–1530

Torney F, Trewyn BG, Lin VS-Y, Wang K (2007) Mesoporous silica nanoparticles deliver DNA and chemicals into plants. Nat Nanotech 2:295–300. doi:10.1038/nnano.2007.108

Triantaphylidès C, Krischke M, Hoeberichts FA, Ksas B, Gresser G, Havaux M, van Breusegem F, Mueller MJ (2008) Singlet oxygen is the major reactive oxygen species involved in photooxidative damage to plants. Plant Physiol 148:960–968. doi:10.1104/pp.108.125690

van Hoecke K, de Schamphelaere KAC, Ramirez-Garcia S, van der Meeren P, Smagghe G, Janssen CR (2011) Influence of alumina coating on characteristics and effects of SiO_2 nanoparticles in algal growth inhibition assays at various pH and organic matter contents. Environ Int 37:1118–1125. doi:10.1016/j.envint.2011.02.009

641 Vivero-Escoto JL, Huxford-Phillips RC, Lin W (2012) Silica-based nanoprobes for biomedical
642 imaging and theranostic applications. Chem Soc Rev 41:2673–2685.
643 doi:10.1039/C2CS15229K
644 Zhang X, Wollenweber B, Jiang D, Liu F, Zhao J (2008) Water deficits and heat shock effects on
645 photosynthesis of a transgenic *Arabidopsis thaliana* constitutively expressing *ABP9*, a bZIP
646 transcription factor. J Exp Bot 59:839–848. doi:10.1093/jxb/erm364

FIGURE CAPTIONS

Fig. 1 *A. thaliana* cell biomass concentration (g fresh weight mL^{-1}) (**a**–**c**) and cell viability (**d**–**f**). ACSC were treated with CMB@SiO_2 (**a**, **d**), nSiO_2 (**b**, **e**) and CMB clusters (**c**, **f**) at different concentrations for 3, 24 and 72 hours. Relative cell viability is expressed as percentage related to control at each time point. * Significant differences between nanomaterial treatment and control ($p < 0.05$)

Fig. 2 ACSC chlorophyll (**a**–**c**) and carotenoid (**d**–**f**) contents (μg g^{-1} dry weight), and PSII maximum quantum yield (F_v/F_m) (**g**–**i**). ACSC were treated with CMB@SiO_2 (**a**, **d**, **g**), nSiO_2 (**b**, **e**, **h**) and CMB clusters (**c**, **f**, **i**) at different concentrations for 3, 24 and 72 hours. * Significant differences between nanomaterial treatment and control ($p < 0.05$)

Fig. 3 Level of lipid peroxidation in *A. thaliana* cells. ACSC were treated with CMB@SiO_2 (**a**), nSiO_2 (**b**) and CMB clusters (**c**) at different concentrations for 3, 24 and 72 hours. TBARS content is expressed as percentage related to control at each time point. * Significant differences between nanomaterial treatment and control ($p < 0.05$)

Fig. 4 Antioxidant enzymatic activities in *A. thaliana* cells. ACSC were treated with CMB@SiO_2 (**a**, **d**, **g**, **j**, M), nSiO_2 (**b**, **e**, **h**, **k**, **n**) and CMB clusters (**c**, **f**, **i**, **l**, **o**) at different concentrations for 3, 24 and 72 hours. Different letters above bars indicate statistical significance ($p < 0.05$) at each time point

Fig. 5 TEM images of *A. thaliana* cells in culture medium after 72 hours of treatment with 60 mg L^{-1} CMB clusters (**a**, **d**), 100 mg L^{-1} CMB@SiO_2 (**b**, **e**), and 100 mg L^{-1} nSiO_2 (**c**, **f**). The cell wall (CW), and the nanomaterials outside (black arrows) and inside cells, cell wall or vesicles (white arrows) are shown

Figure 1

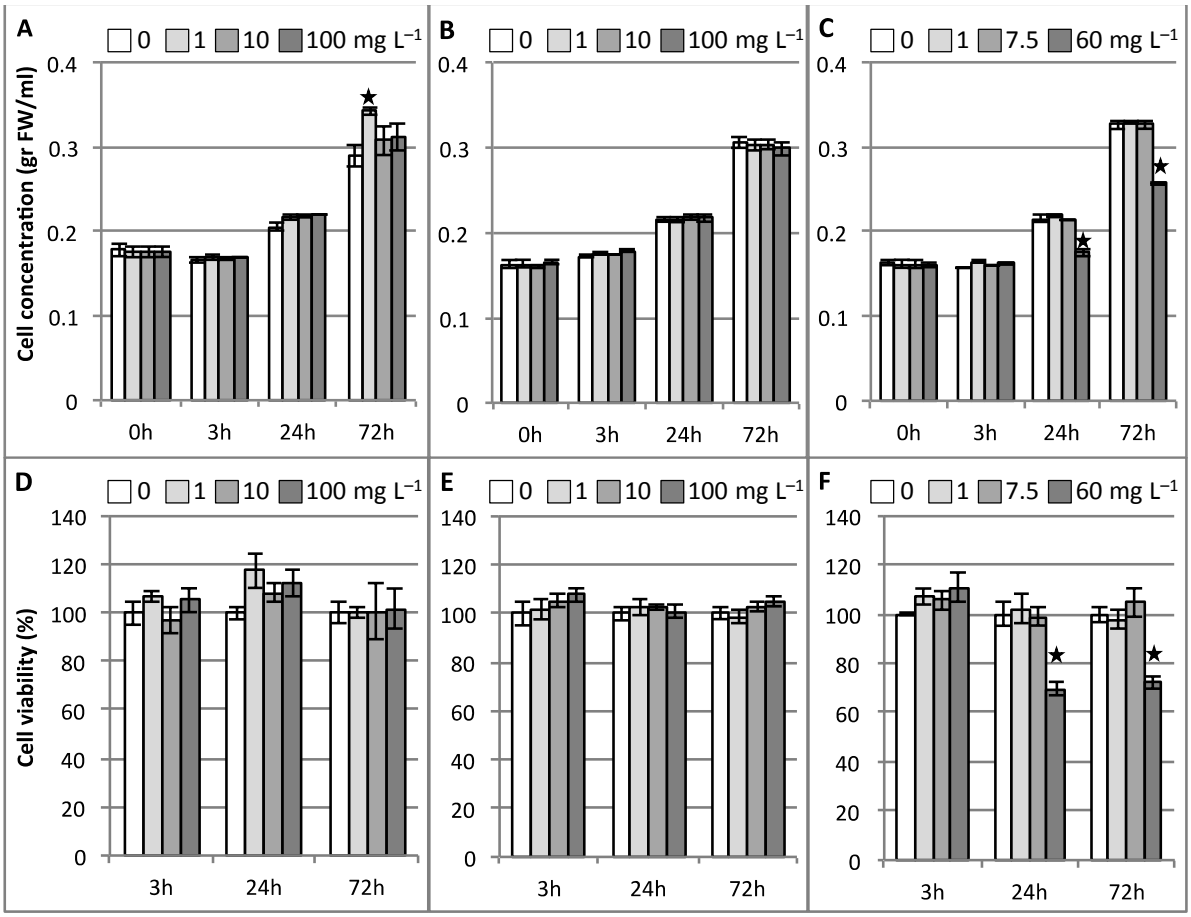

Fig. 1

Figure 2

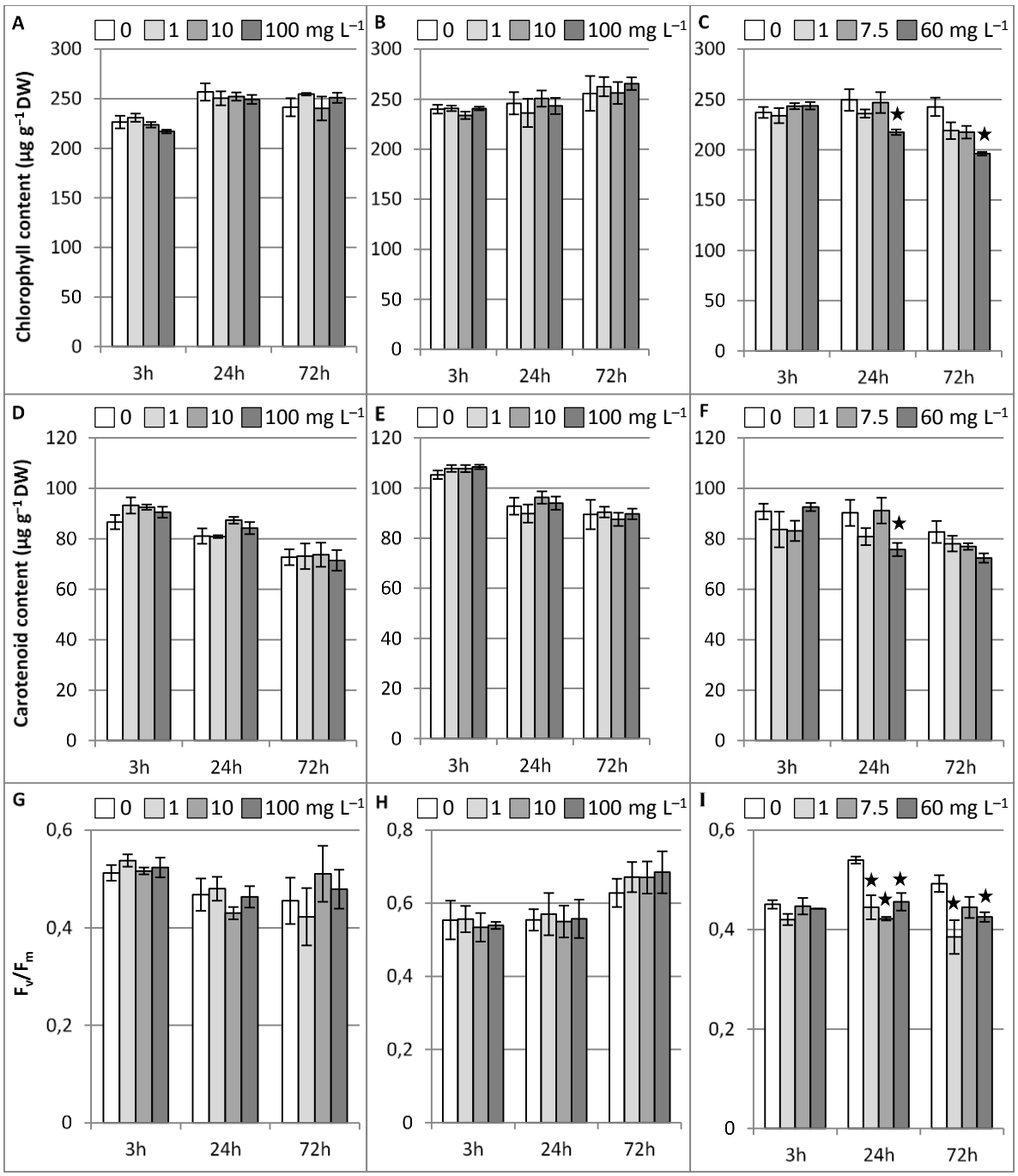
A
B
C
D
E
F
G
H
I
0 1 10 100 mg L−1
0 1 7.5 60 mg L−1
Chlorophyll content (µg g−1 DW)
Carotenoid content (µg g−1 DW)
Fv/Fm
3h
24h
72h

Figure 3

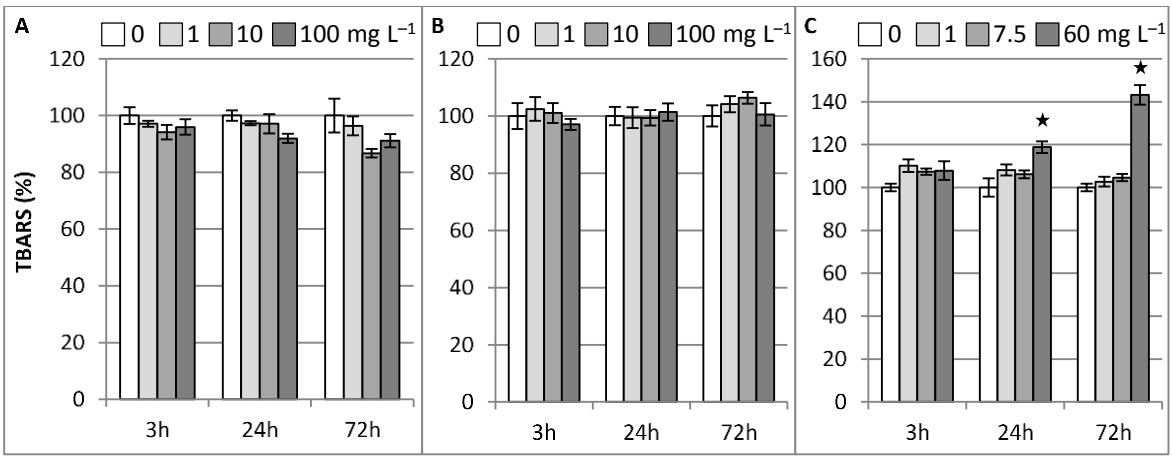
A
0
1
10
100 mg L−1
TBARS (%)
120
100
80
60
40
20
0
3h
24h
72h
B
0
1
10
100 mg L−1
120
100
80
60
40
20
0
3h
24h
72h
C
0
1
7.5
60 mg L−1
160
140
120
100
80
60
40
20
0
3h
24h
72h

Figure 4

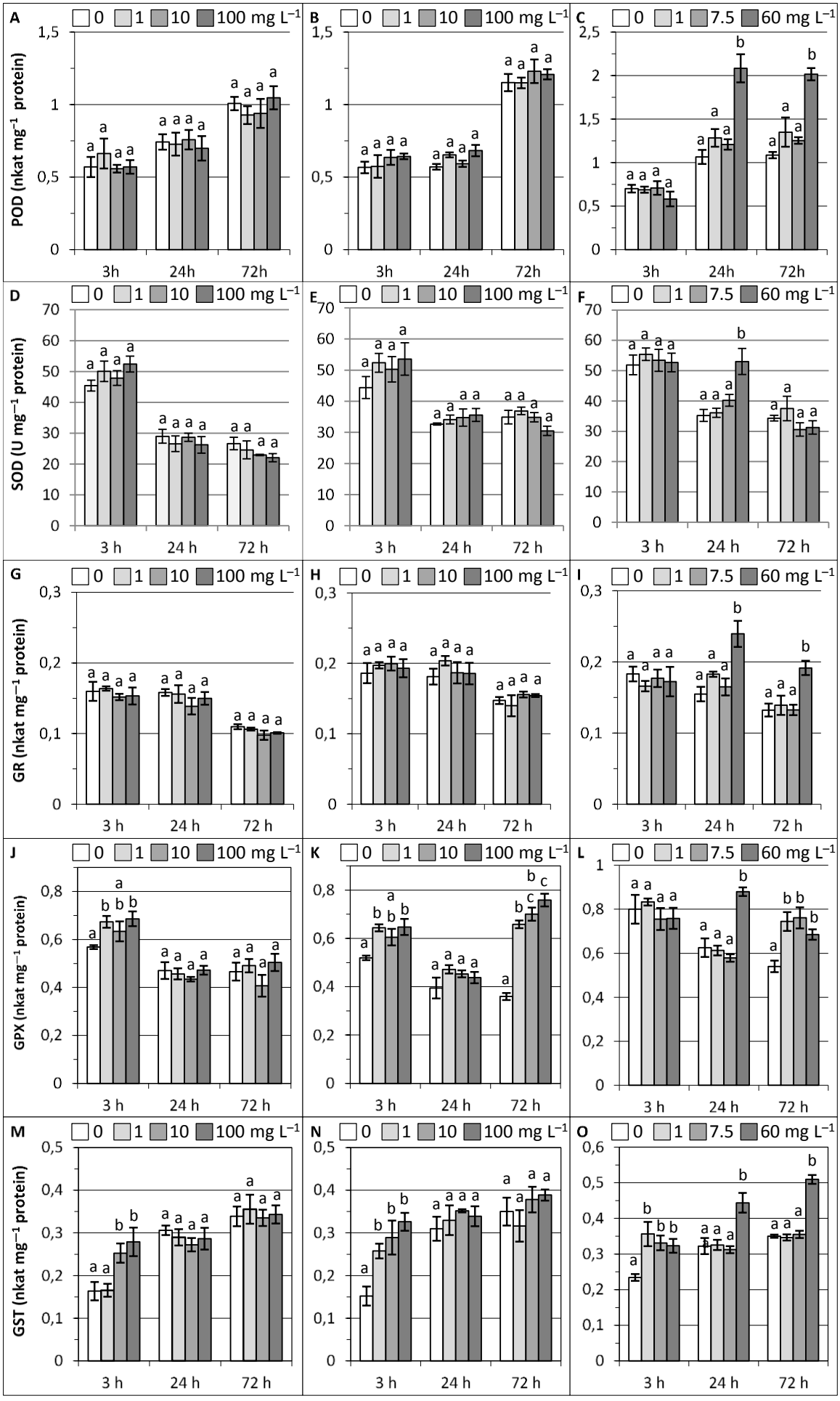
A
B
C
D
E
F
G
H
I
J
K
L
M
N
O
0
1
10
7.5
100 mg L−1
60 mg L−1
POD (nkat mg−1 protein)
SOD (U mg−1 protein)
GR (nkat mg−1 protein)
GPX (nkat mg−1 protein)
GST (nkat mg−1 protein)
3h
24h
72h
3 h
24 h
72 h

Figure 5

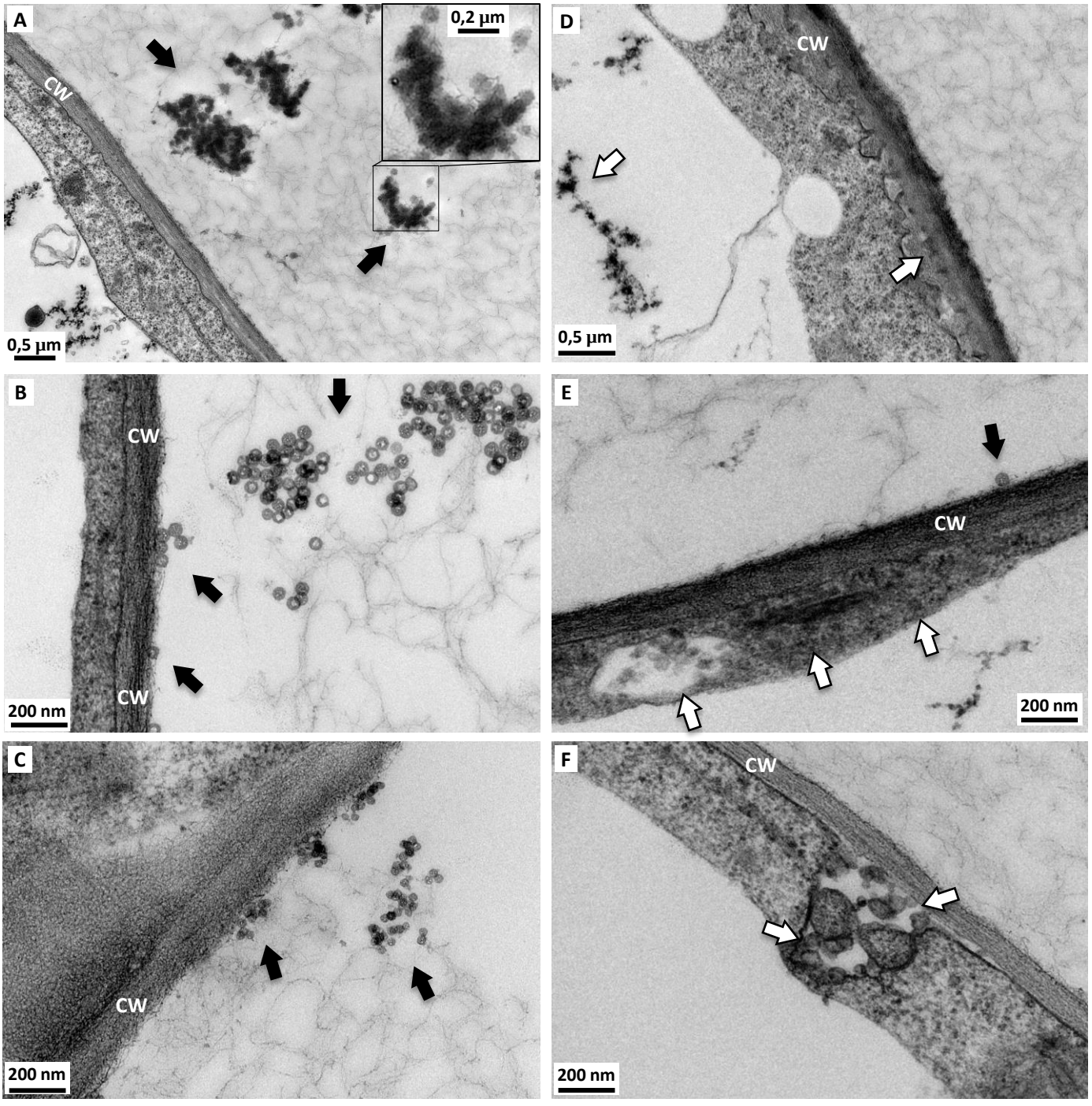

Fig. 5